Int. J. Materials and Product Technology, Vol. 39, No 1/2, p. 195-204 (2010)

Effect of Grain Size and Hydrogen Passivation on the Electrical Properties of Nanocrystalline Silicon Films

M. F. Cerqueira[1], T.V. Semikina[1], N. V. Baidus[1], E. Alves[2]

[1]Centro de Física, Universidade do Minho, 4710-057 Braga, Portugal
[2]Instituto Técnico Nuclear (ITN), EN 10, 2686-953 Sacavém, Portugal

Abstract: The properties of mixed-phase (nanocrystalline/amorphous) silicon layers produced by reactive RF-sputtering are described. The chemical composition and nanostructure [i.e. nanocrystal (NC) size and volume fraction] of the films were studied by Rutherford backscattering spectroscopy (RBS) and micro-Raman spectroscopy, respectively. Samples with different fractions of the nanocrystalline phase and NC mean size were produced by changing the deposition parameters, without post-growth annealing. The electrical conductivity of the films, measured as function of temperature, is discussed in relation to their nanostructure.

Keywords: amorphous silicon; nanocrystal; Raman spectroscopy; electrical properties.

1. INTRODUCTION

Intrinsic and Er-doped nanocrystalline silicon (nc-Si) have been attracting high interest of researchers as promising candidates for the realization of Si-based visible and infrared light sources, in particular, for optical communication systems [1]. This interest has been increased by the recent development of all-Si Raman laser [2] and the observation of strong enhancement of the Raman scattering intensity in nc-Si as compared to the bulk material [3]. For any device application, the electrical properties of the produced material are of utmost importance and there is a need of developing an inexpensive technology of fabrication of nc-Si with controlled optical and electrical properties.

Hydrogenated nanocrystalline silicon (nc-Si:H) possesses higher electrical conductivity, compared to amorphous silicon (a-Si), while its preparation, in the form of thin films, is still inexpensive. It is known that the electrical conductivity [4], as well as other physical properties relevant for many applications [5], is strongly influenced by the film's nanostructure, but from physical point of view, many questions remain unclear [6]. In this paper we describe the results of experiments performed in order to obtain new data concerning the influence of the nanostructure (namely, nanocrystal mean size and volume fraction of the crystalline phase) and chemical composition (hydrogen content) of nc-Si:H films produced by RF magnetron sputtering on their electrical properties.

2. EXPERIMENTAL DETAILS

Nc-Si:H films were grown by reactive magnetron sputtering of Si targets in an Ar/H_2 atmosphere and deposited onto glass substrates at a fixed RF sputtering power of 80W. Details of the growth procedure have been described in Ref. [7]. Samples with different nanostructures and hydrogen contents were obtained by changing deposition parameters, namely, the substrate temperature (T_g) and the hydrogen flow rate in the deposition chamber during the films growth process, the latter defined as $R_{H_2} = F(H_2)/[F(H_2) + F(Ar)] \times 100\%$, where the F designates the corresponding gas-flow rates. The growth parameters for all the samples produced and studied in this work are presented in Table I. The typical thickness of the films was 500nm.

The chemical composition of the films was determined by a combination of the Rutherford Backscattering Spectroscopy (RBS) and Elastic Recoil Detection (ERD) techniques. The hydrogen contents in the samples are presented in Table I. Samples #28, #33 and #34 were grown in a hydrogen-rich atmosphere and the RBS/ERD analysis indeed indicates a high amount of hydrogen in the films ($\geq$20 at %). Samples #48, #07 and #11 were grown in a low hydrogen atmosphere and are

characterised by a lower hydrogen content (around 2.5 at %). Two more samples (#26 and #32) were produced under intermediate hydrogen dilution in argon.

Table I – Growth conditions, hydrogen atomic concentration, nanostructure parameters, RT conductivity, and parameters of the temperature dependence of the conductivity for the samples produced and studied in this work.

Sample	T_g, °C	R_{H_2}, %	H, at %	D, nm	c, %	$\sigma_d(300\text{K})$, $\Omega^{-1}\text{cm}^{-1}$	σ_0, $\Omega^{-1}\text{cm}^{-1}$	E_a, eV
#07	350	17	2.2	7	40	$4.6\cdot10^{-8}$	5.31	0.48
#11	350	37	3	8	60	$2.6\cdot10^{-1}$	18.1	0.11
#26	350	47	7.5	8	70	$1.4\cdot10^{-3}$	-	-
#28	350	63	20	7	40	$4.7\cdot10^{-8}$	-	-
#32	300	47	7.5	8	70	$2.5\cdot10^{-2}$	-	-
#33	25	63	27.5	<3	<20	$1.6\cdot10^{-11}$	$3.14\cdot10^{5}$	0.97
#34	50	63	25.8	<3	<20	$1.0\cdot10^{-10}$	-	-
#48	300	37	3	6	30	$7.9\cdot10^{-7}$	2.80	0.39

Our previous Transmission Electron Microscopy (TEM) studies [8] have shown that silicon films contain both nanocrystalline and amorphous phases. In this work, the nanocrystal (NC) size, *D*, and the volume fraction, *c*, were determined from micro-Raman spectra recorded under excitation with the 514.5 nm line of an Ar^+ laser, through the analysis of the characteristic phonon modes. For the (dark) conductivity measurements, thermally evaporated coplanar Al contacts were used, with a gap of 0.5 mm between the electrodes. The measurements were performed in vacuum at temperatures ranging from 200 to 300 K. These results are presented and discussed below.

3. RESULTS AND DISCUSSION

3.1 Crystalline fraction characterisation by Raman spectroscopy

Figure 1 shows several Raman spectra measured for the studied samples. Curve A was obtained for samples #33 and #34; curve B for sample #48, curve C represents samples #11, #26 and #32 and curve D is characteristic of samples #07 and #28. The broad band around 480 cm^{-1} is related to the amorphous silicon matrix and is present in all the spectra of Fig. 1. The presence of Si nanocrystals is visible in the Raman spectra B, C and D by the relatively narrow peak in the vicinity of 520 cm^{-1}. This asymmetric peak is related to the transverse-longitudinal optical (TO-LO) confined phonon modes of nanocrystalline silicon. Within a model considering phonon confinement in a crystalline nanoparticle, the peak position (ω_0) shifts to smaller wave numbers for decreasing NC size and the asymmetry (associated with the contribution of the confined phonon overtones) increases [9]. Such models have been proved to work quite well for NCs embedded in a foreign matrix, e.g. CdSe in glass [9] where a well defined barrier for optical phonons exists. It is perhaps less obvious that strong confinement models can apply to systems like nc-Si/a-Si where barriers between the crystalline core and the matrix are random, however, the sufficiently large difference that exists between the peaks of the phonon densities of states for c-Si (521 cm^{-1}) and a-Si (480 cm^{-1}, see [10] for recent calculated results) makes it reasonable to assume that the relative displacement of two Si atoms vanishes at the NC matrix interface, at least for the first quantified phonon modes. Considering the perfect confinement of the optical phonon in a spherical shape[1] NC, the mean diameter can be evaluated from the relation [9, 11],

$$D = 2\xi_1\left[\left(\omega_{TO-LO} - \omega_0\right)/\beta_{LO}\right]^{-1/2} \qquad (1)$$

[1] The approximately spherical shape of the NCs was confirmed by our previous TEM studies.

where $\xi_1 \approx 4.49$ is the first root of the spherical Bessel function j_1, ω_{LO-TO} is the bulk TO-LO phonon frequency and β_{LO} is the curvature parameter of the LO phonon branch of bulk c-Si[2]. Unfortunately, for NCs larger than ≈ 6 nm, the shift $(\omega_{TO-LO} - \omega_0)$ is too small to be reliably determined from the experimental spectra and the use of Eq. (1) is hardly possible. Still, one can estimate the NC size from the peak asymmetry, although this is more involving since it requires modelling of the lineshape and the broadening is not only due to the contribution of phonon overtones in each NC but also because of the NC size dispersion. Nevertheless, it is possible to obtain reasonably good fits to the nc-Si peak using the model explained in Ref. [11] (taking into account only the short-range part of the electron-phonon interaction) as shown in Fig. 2. This way we determined the NC mean size for the (most crystalline) samples #07 and #28.

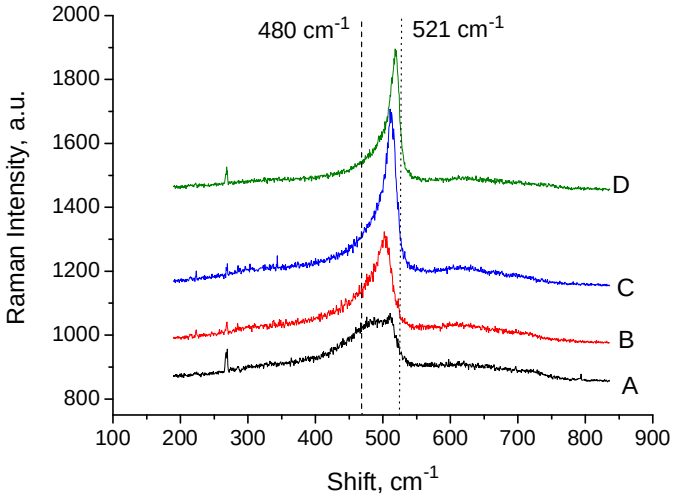

Figure1: Raman spectra of the nc-Si/a-Si samples listed in Table I (A = #33, 34; B = #48; C = #11, 26, 32; D = #07, 28).

[2] The curvature parameter was calculated using a parabolic approximation of the LO phonon dispersion curve, with the Brillouin zone centre (edge) value of 521 cm^{-1} (375 cm^{-1}).

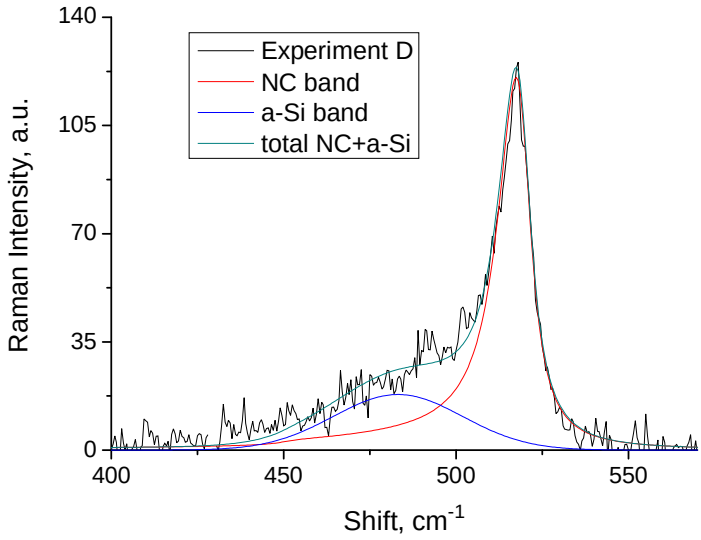

Figure2: Fitting of the Raman spectrum of the sample #07 (curve D in Fig. 1) with model of Ref. [11] using the NC mean size of 8 nm and standard deviation of 10% plus a Gaussian with 80cm^{-1} of FWHM and centred at 480 cm^{-1} representing the a-Si contribution.

The Raman spectra of samples #33 and #34 (curve A in Fig. 1), grown at low temperature, almost do not show the crystalline peak and are dominated by the broad amorphous band. We used a Gaussian function to model this band. As it is known, the maximum position and the width of the band depend on the hydrogen concentration and other growth conditions and the typical values are 470 - 480 cm^{-1} and 80 - 100 cm^{-1}, respectively [12]. Our fitted Gaussian parameters also fall in these ranges.

The relative weight of the amorphous and crystalline bands in the Raman spectra is commonly used in order to estimate the volume fraction of the crystalline phase, c, through the following phenomenological relation [13 - 15]:

$$c = I_c / \left(I_c + y I_a \right) \tag{2}$$

where I_c and I_a are the integrated intensities of the bands produced by the crystalline and amorphous phases, respectively, and y is an empirical parameter of the order of unity. Although the values of y

that have been used for mixed-phase silicon vary considerably, the most recent data indicate that $1 < y < 2$ [14, 15]. In this work we used $y = 1.7$ [15]. The obtained values of D and c are presented in Table I. For samples #33 and #34, the NC size and the volume fraction of the crystalline phase were estimated from TEM images.

As one might expect, increasing the substrate temperature from 25-50^{o}C to 300-350^{o}C leads to the formation of larger crystallites with higher c because the higher substrate temperature enhances the mobility of the sputtered atoms on the growing surface.

3.2 Electrical conductivity

The room temperature (RT) values of the conductivity (σ_d) for all samples are shown in Table I. We obtained σ_d ranging from $1.6 \cdot 10^{-11}\ \Omega^{-1}\text{cm}^{-1}$ (which is a typical value for a-Si:H) to $2.6 \cdot 10^{-1}\ \Omega^{-1}\text{cm}^{-1}$ (a typical value for nanocrystalline silicon [16]). The lowest conductivity was measured for the samples with few (c<20%) and small size (D<3nm) crystallites (Raman spectrum A in Fig. 1). The highest σ_d values were obtained for the samples that show the Raman curve D (samples #26, #11 and #32), i.e. those with high c and large D. Figure 3 shows the variation (namely, the increase) of the RT conductivity with the degree of crystallinity of the sample. So, is it only the material's nanostructure that determines the behaviour of RT dark conductivity or does the hydrogen content also play a role?

Samples #48 and #11 with practically the same chemical composition show substantially different σ_d values. The main difference between these samples is the crystalline volume fraction and the average NC size. Furthermore, the σ_d values of samples #07 and #28 with similar microstructure parameters (c and D) but quite different hydrogen contents are similar. Thus, the nanostructure seems to be the key factor to determine the RT conductivity. However, if we compare samples #26 and #11 with

approximately the same NC size and crystalline volume fraction, they have rather different σ_d values. The difference between these two samples is mostly the hydrogen content, and, for these samples the conductivity value increases when the hydrogen content in the film decreases from 7.5 to 3 at%. The same tendency is observed for samples #34 and #33. Therefore we have to be cautious concerning the effect of hydrogen addition on the electrical transport in the mixed-phase films. Our results indicate that the nanostructure is the main factor influencing the dark conductivity but in certain cases the hydrogen content also seems to play an important role. It is well known that the hydrogen is essential for the growth of good quality amorphous silicon since it improves its optical and electrical properties by saturating the dangling bonds (DBs). According to our results, it can be concluded that a small amount of hydrogen (≈ 3 at %) is enough for the DB saturation (note the high σ_d value for sample #11 in Table I). The extra hydrogen may form complexes that lead to the deterioration of the electrical conductivity by decreasing the carrier mobility.

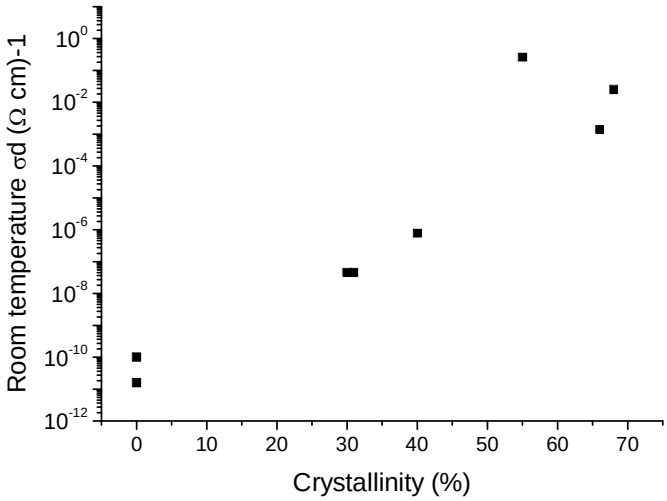

Figure 3: Measured RT conductivity values versus volume fraction of the nanocrystalline phase in the sample as determined from the Raman spectra.

In order to understand the mechanism of the electrical conductivity in the mixed-phase Si films it is important to determine its temperature dependence. For all our samples the variation of σ_d with temperature (T) can be approximated by the Arrhenius equation:

$$\sigma_d(T) = \sigma_0 \exp[-E_a/(kT)] \tag{3}$$

where σ_0 is a constant, E_a is an activation energy, k is the Boltzmann constant. Usually the interpretation of Eq. (3) for disordered materials is the following: E_a is equal to the energy difference between the mobility edge and the Fermi level at $T = 0$ and the pre-factor σ_0 is characteristic of the carrier transport through the extended states. Applying Eq. (3) to our data we extracted the values of σ_0 and E_a that are presented in Table I. Notice that the activation energy changes from 0.97 to 0.11 eV when the RT conductivity changes by ten orders of magnitude (from $1.6 \cdot 10^{-11}\ \Omega^{-1}\text{cm}^{-1}$ to $2.6 \cdot 10^{-1}\ \Omega^{-1}\text{cm}^{-1}$). Since E_a and $\sigma_d(300\text{K})$ vary in a correlated way (the activation energy is lower for samples with higher RT conductivity), we suggest that, among the samples #48, #07 and #11, this is just due to a different position of the Fermi level with respect to the bottom of the conduction band of the nanocrystalline phase. According to the considerably higher σ_0 and E_a values, the conductivity in the sample #33 occurred mainly through the amorphous phase. Figure 4 shows the comparison of the correlation between σ_0 and E_a obtained from our experimental data with the empirical Meyer-Neldel rule [17, 18],

$$\sigma_0 = A\exp(E_a/E_0) \tag{4}$$

where A and E_0 are some positive constants. Even though not well-understood, this relationship has been consistently verified for disordered semiconductors [19]. Meyer-Neldel parameters values of

0.035 eV for E_0 and 10^{-6} Ω^{-1}cm^{-1} for A have been obtained by Monte Carlo simulations for a-Si:H [20]. For microcrystalline silicon, the values of E_0 = 0.06 eV and A=10^{-2} Ω^{-1}cm^{-1} have been reported [21]. The parameters E_0 and A of Eq. (4) are represented by the straight lines in Fig. 4, for both amorphous and microcrystalline materials. It can be seen from Fig. 4 that the experimental data obey the Meyer-Neldel rule except for the sample #11. It looks natural that the sample #33 containing a low fraction of small Si crystallites (Raman curve A) fits the line corresponding to a-Si. On the contrary, the samples #7 and #48 (with Raman curves B and C) follow the trend characteristic of microcrystalline Si. This is compatible with the relatively high NC volume fraction in both samples, above the percolation threshold, so that the conductivity can occur through the crystalline phase and by hopping over (low) barriers formed on the grain boundaries. The sample #11 (Raman curve D in Fig. 1) is considerably above the line corresponding to microcrystalline Si, even though the conductivity of this sample must be completely dominated by the crystalline phase ($c \approx 60\%$). One possible reason for this can be an unintentional doping of this sample, leading to the lower E_a and higher conductivity.

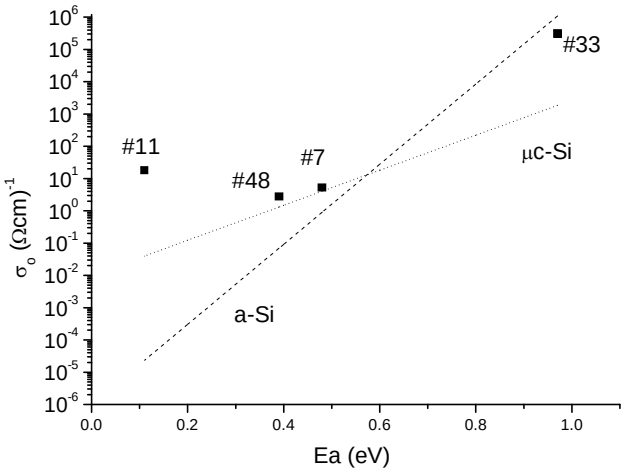

Figure 4: Meyer-Nelder plot of the conductivity activation energy versus pre-exponential factor (σ_0) for several samples. Straight lines represent a-Si:H and μc-Si:H according to the data from the literature [20, 21].

4. Conclusion

We have shown the ability to produce by RF-sputtering amorphous and nanocrystalline silicon layers, without the need to perform any high-temperature annealing in order to form Si NCs. The average size of NCs embedded in a matrix of amorphous Si and the volume fraction of the crystalline phase, have been determined using the Raman spectroscopy data. The films with high c show high RT conductivity values, increasing with the NC volume fraction, and are characterized by small activation energies of the $\sigma_d(T)$ dependence. This findings support the idea that, in this kind of mixed-phase materials, the electrical transport is essentially due to the nanocrystalline component. When the crystalline phase fraction reaches 30-35 %, there is a sharp increase in the conductivity that can be associated with the geometrical percolation threshold. We have also shown that there is an optimum concentration of hydrogen in the gas chamber, approximately (25 ± 5) %. The excess of hydrogen leads to the formation of additional hydrogen complexes with a deterioration of the conductivity.

Acknowledgments

This work was supported by a FCT Project POCTI/CTM/39395/2001. We would also like to thank Professor G. J. Adriaenssens from Department Natuurkunde, K.U. Leuven (Belgium) for help with experiments and to Prof Mikhail Vasilevskiy from Physics Department of U. Minho for the useful discussions.

References

[1] – S. Coffa and L. Tsybeskov (Ed.), "Silicon-Based Optoelectronics", MRS Bulletin 23 (1998) 16.

[2] – H.S. Rong, A.S. Liu, R. Jones, O. Cohen, D. Hak, R. Nicolaescu, A. Fang and M. Paniccia, Nature 433 (2005) 292.

[3] – L. Cao, B. Nabet and J. E. Spanier, Phys. Rev. Lett. 96 (2006) 157402.

[4] – Y. Kanzawa, T. Kageyama, T. Takeoka, M. Fujii, S. Hayashi and K. Yamamoto, Solid State Commun. 102 (1997) 533.

[5] – S. Veprek, F. A. Sarott and Z. Iqbal, Phys. Rev. B 36 (1987) 3344.

[6] – L. Pavesi, Materials Today (2005) 18

[7] – M. F. Cerqueira, M. Andritschky, L. Rebouta, J. A. Ferreira and M. F. da Silva, Vacuum 46 (1995) 1385.

[8] – M. Losurdo, M. M. Giangregorio, P. Capezzuto, G. Bruno, M. F. Cerqueira and E. Alves, Appl. Phys. Lett. 82 (2003) 2993.

[9] – A. G. Rolo and M. I. Vasilevskiy, J. Raman Spectr. 38 (2007) 618.

[10] – S. M. Nakhmanson, P. M. Voyles, N. Mousseau, G. T. Barkema and D. A. Drabold, Phys. Rev. B 63 (2001) 235207.

[11] – M. I. Vasilevskiy, A. G. Rolo, M. J. M. Gomes, O. V. Vikhrova and C. Ricolleau, J. Phys.: Condensed Matter 13 (2001) 3491.

[12] – S. T. Kshirsagar, R. O. Dusane and V. G. Bhide, Phys. Rev. B 40 (1989) 8026.

[13] – R. Tsu, J. Gonzalez-Hernandez, S. S. Chao, S. C. Lee and K. Tanaka, Appl. Phys. Lett. 40 (1982) 534.

[14] – M. Ledinsky, L. Fekete, J. Stuchlik, T. Mates, A. Fejfar and J. Koška, J. Non-Cryst. Solids 352 (2006) 1209.

[15] – E. Vallat-Sauvain, C. Droz, F. Meillaud, J. Bailat, A. Shah and C. Ballif, J. Non-Cryst. Solids 352 (2006) 1200.

[16] – Xi-wen Zhang and Gao-rong Han, Thin Solid Films, 415 (2002) 5.

[17] – W. Beyer and H. Overhof, in: J. I. Pankove (ed.), “Hydrogenated Amorphous Silicon”, Vol. 21C, Academic Press, New York (1984) p. 257.

[18] – W. Meyer and H. Neldel, PHYSIKALISCHE ZEITSCHRIFT 12 (1937) 588.

[19] – N. F. Mott, E. A. Davies, “Electronic Processes in Non-Crystalline Materials”, Oxford: Clarendon (1979)

[20] – W. C. Chen, L. Hamel and A. Yelon, J. Non-Cryst. Solids 220 (1997) 254.

[21] – F. Demichelis, C. F. Pirri and E. Tresso, Philosophical Magazine B 67 (1993) 331.